Contribution of Surface Salt Bridges to Protein Stability[†,‡]

Pavel Strop[§] and Stephen L. Mayo*[,||]

Biochemistry Option, California Institute of Technology, Mail Code 147-75, Pasadena, California 91125, and Howard Hughes Medical Institute and Division of Biology, California Institute of Technology, Mail Code 147-75, Pasadena, California 91125

Received September 27, 1999; Revised Manuscript Received November 16, 1999

ABSTRACT: The role of surface salt bridges in protein stabilization has been a source of controversy. Here we present the NMR structure of a hyperthermophilic rubredoxin variant (PFRD-XC4) and the thermodynamic analysis of two surface salt bridges by double mutant cycles. This analysis shows that the surface side chain to side chain salt bridge between Lys 6 and Glu 49 does not stabilize PFRD-XC4. The main chain to side chain salt bridge between the N-terminus and Glu 14 was, however, found to stabilize PFRD-XC4 by 1.5 kcal mol^{-1}. The entropic cost of making a surface salt bridge involving the protein's backbone is reduced, since the backbone has already been immobilized upon protein folding.

Proteins from thermophilic organisms offer good model systems with which to address the origins of thermostability. Several trends were found to be associated with increased thermal stability. These trends include increased packing density, increased core hydrophobicity, decreased length of surface loops, and improved secondary structure stabilization such as N-terminal and C-terminal helix capping (*1*). Comparison of many thermophilic proteins also indicates a high level of occurrence of surface electrostatic interactions relative to mesophilic homologues (*1*−*6*). Buried salt bridges and salt bridges at dimer interfaces as well as surface salt bridges have been reported to contribute to the increased stability of proteins (*7*−*11*). These findings appear to contradict other thermodynamic evidence which shows that surface ion pairs make little contribution to protein stability (*12*−*14*).

It has been difficult to study hyperthermophilic proteins by thermodynamic analysis, since most of the known hyperthermophilic proteins do not unfold reversibly (*15*−*23*). We previously designed a *Pyroccocus furiosus* rubredoxin variant (PFRD-XC4)[1] to eliminate the iron-binding site using a computational design algorithm. The iron-binding site in wild-type rubredoxin is thought to be the cause of its irreversible unfolding (*22*). The mutations for PFRD-XC4 are C5L, C8T, C38A, and C41T. PFRD-XC4 is able to fold in the absence of iron, undergoes reversible denaturation, and has a melting temperature of 82 °C (*24*). The variant provides an excellent opportunity for systematic exploration of the factors determining protein thermostability.

The NMR solution structure of PFRD-XC4 reveals a fold similar to that of wild-type *P. furiosus* rubredoxin (PFRD). Given that PFRD-XC4 adopts a fold similar to that of PFRD and undergoes reversible unfolding, the importance of interactions that are responsible for the extreme stability of PFRD can now be addressed. Two interactions found in PFRD, but not in mesophilic rubredoxins, have been proposed to contribute to its hyperthermostability (*5*, *25*). These are the salt bridges between the N-terminus and the side chain of Glu 14 and between the side chains of Lys 6 and Glu 49. Here we present the NMR solution structure of PFRD-XC4 and thermodynamic analysis of the two salt bridges by double mutant cycles.

MATERIALS AND METHODS

Mutagenesis and Protein Purification. The hyperthermophilic variant PFRD-XC4 and all PFRD-XC4 mutants were constructed by inverse PCR (*26*) using a synthetic *P. furiosus* rubredoxin gene in plasmid pt7-7 (*27*). The mutations for PFRD-XC4 are C5L, C8T, C38A, and C41T. All mutants were verified by sequencing. Recombinant proteins were expressed by IPTG induction in BL21(DE3) hosts (Invitrogen) as described previously (*28*) and isolated using a freeze−thaw method (*29*). Purification was accomplished by reverse-phase high-performance liquid chromatography using first a linear 1%/min followed by a 0.07%/min acetonitrile/water gradient containing 0.1% TFA. Molecular weights were verified by mass spectrometry.

NMR Structure Determination. NMR data were collected on a Varian Unity Plus 600 MHz spectrometer equipped with a Nalorac inverse probe with a self-shielded *z*-gradient. NMR samples were prepared in 90/10 H_2O/D_2O or 99.9% D_2O with 200 mM NaCl and 25 mM sodium acetate-d_3 (pH 6.3). The sample concentration was approximately 1.5 mM. Sequential assignment of resonances was achieved by

[†] This work was supported by the Howard Huges Medical Institute (S.L.M.) and a NSF fellowship (P.S.).

[‡] The coordinates for the structure have been deposited in the Protein Data Bank (file 1qcv).

* To whom correspondence should be addressed. E-mail: steve@mayo.caltech.edu. Telephone: (626) 395-6408. Fax: (626) 568-0934.

[§] Biochemistry Option, California Institute of Technology.

[||] Howard Hughes Medical Institute and Division of Biology, California Institute of Technology.

[1] Abbreviations: NMR, nuclear magnetic resonance; PFRD, *P. furiosus* rubredoxin; PFRD-XC4, *P. furiosus* rubredoxin variant with C5L, C8T, C38A, and C41T mutations; NOE, nuclear Overhauser enhancement; CD, circular dichroism; T_m, midpoint of the thermal unfolding transition; ΔG_u, free energy of unfolding; *m* value, slope of ΔG_u versus denaturant concentration; GdmCl, guanidinium chloride.

10.1021/bi992257j CCC: $19.00
Published on Web 00/00/0000 PAGE EST: 5

Table 1: NMR Structure Statistics

No. of Distance Restraints	
intraresidue	162
sequential	96
short-range ($\|i - j\| = 2-5$ residues)	80
long-range ($\|i - j\| > 5$ residues)	114
hydrogen bond	20
ϕ	22
total	494

Structural Statistics rms deviation	$\langle SA \rangle^a \pm SD^b$	$(SA)_r^d$
distance restraint (Å)	0.031 ± 0.003	0.019
idealized geometry		
bonds (Å)	0.0039 ± 0.0002	0.0019
angles (deg)	0.64 ± 0.02	0.52
impropers (deg)	0.44 ± 0.02	0.37

Structural Statistics atomic rms deviation (Å)	$\langle SA \rangle$ vs $SA^c \pm SD$
backbone (residues 1−51)	1.02 ± 0.05
heavy atoms (residues 1−51)	1.42 ± 0.04
backbone (residues 1−36 and 47−51)	0.52 ± 0.02
heavy atoms (residues 1−36 and 47−51)	0.97 ± 0.03
atomic rms deviations between PFRD and PFRD-XC4 backbone (residues 1−36 and 47−51)	1.18

[a] $\langle SA \rangle$ are 28 simulated annealing structures. [b] SD is the standard deviation. [c] SA is the average structure. [d] $(SA)_r$ is the minimized average structure.

standard homonuclear methods (*30*). Two-dimensional DQF-COSY (*31*), TOCSY (*32*), and NOESY (*33*) spectra were acquired at 25 °C. The TOCSY spectrum was recorded with an 80 ms mixing time using a clean-MLEV17 mixing sequence. NOESY spectra were acquired with a 150 ms mixing time for use during resonance assignments and a 100 ms mixing time to derive distance restraints. Water suppression was accomplished either with presaturation during the relaxation delay or with pulsed field gradients (*34*). Spectra were processed with VNMR (Varian Associates) and were assigned with ANSIG (*35*). NOEs were classified into three distance-bound ranges based on cross-peak intensity: strong (1.8−2.7 Å), medium (1.8−3.3 Å), and weak (1.8−5.0 Å). Upper bounds for restraints involving methyl protons were increased by 0.5 Å to account for the increased intensity of methyl resonances. Partially overlapped NOEs were set to weak restraints. Hydrogen bonds were defined on the basis of the presence of supporting NOE peaks and by association with slowly exchanging backbone amide protons (protection factors ≥ 100). Distance restraints for the hydrogen bonds were as follows: $r_{NH-O} = 1.5-2.8$ Å and $r_{N-O} = 2.4-3.5$ Å. Dihedral restraints were defined on the basis of the coupling constants. Residues with a $^3J_{HNHA} \leq 4$ Hz had the ϕ torsional angle restricted to be within the interval of −80° to −40°. Residues with a $^3J_{HNHA} \geq 8$ Hz had the ϕ torsion angle restricted to be within the interval of −160° to −80°. $^3J_{HNHA}$ values were derived from NOESY cross-peak fine structure using the INFIT module of XEASY (*36*).

Structure calculations were performed with X-PLOR (*37*) with the use of standard protocols for hybrid distance geometry-simulated annealing (*38*−*40*). Forty structures were generated and, following regularization and refinement, resulted in an ensemble of 28 structures with no restraint violations of >0.3 Å, rms deviations from idealized bond lengths of <0.004 Å, and rms deviations from idealized bond angles and impropers of <0.65°.

CD Analysis. CD data were collected on an Aviv 62DS spectrometer equipped with a thermoelectric unit and using a 1 cm path length cell. Protein samples were at a concentration of 5 μM in 50 mM sodium phosphate buffer at pH 6.3. Concentrations were determined by UV spectrophotometry. Thermal melts were monitored at 225 nm. Data were collected every 2 °C with an equilibration time of 2 min and an averaging time of 10 s. T_m was determined by fitting the melting curves to a two-state model as described previously (*41*). Guanidinium chloride and urea denaturations were performed at 1 °C. ΔG values, m values, and error estimates were obtained by fitting the denaturation data to a two-state transition as described previously (*42*). GdmCl and urea concentrations were measured by refractometry.

RESULTS AND DISCUSSION

Structure Determination of PFRD-XC4. To ensure that the elimination of the iron center did not change the tertiary fold of PFRD, we determined the solution structure of PFRD-XC4 by standard two-dimensional ^{1}H NMR methods (*30*−*33*). The structure of PFRD-XC4 was determined from 494 experimental restraints (8.3 restraints per residue) that were nonredundant with covalent structure, including 452 NOE distance restraints, 22 dihedral angle restraints, and 20 hydrogen bond restraints (Table 1). Structure calculations were performed using X-PLOR (*37*) and standard protocols for hybrid distance geometry-simulated annealing (*38*−*40*). An ensemble of 28 structures converged with good covalent geometry and no distance restraint violations of >0.3 Å. The data reveal a well-ordered structure except for residues 37−46 with a root-mean-square (rms) deviation from the mean of 0.52 Å for the backbone of residues 1−36 and 47−51. Figure 1a shows the superposition of 28 simulated annealing structures generated using X-PLOR. Residues 37−46 form a loop that is the least ordered region of the structure. In PFRD, the metal binding site is between the two loops formed by residues 5−10 and 37−46, each of which donates two cysteine residues to tetrahedrally coordinate the iron atom (Figure 2). The iron covalently links these two loops and prevents loop mobility. In the PFRD-XC4 structure, one of these loops (residues 37−46) lacks NOE distance restraints and is probably present in multiple conformations.

The stereochemical quality of the ensemble of structures was examined with PROCHECK (*43*). Apart from the glycine residues, 64.2% of the residues are in the most favored regions of ϕ and ψ space, 32.1% in the additional allowed regions, 3.3% in the generously allowed regions, and 0.4% in the disallowed regions. The average backbone structure of PFRD-XC4 superimposes onto PFRD's crystallographic backbone with an rms deviation of 1.2 Å for the backbone of residues 1−36 and 47−51 (Figure 1b).

Stability Studies of PFRD-XC4 Mutants. The salt bridges of interest (between residues 1 and 14 and 6 and 49) are in the well-ordered part of the PFRD-XC4 structure and most likely adopt conformations similar to those in PFRD (Figure 2). A series of mutants were designed to disrupt these salt bridges. The resulting proteins were characterized by both thermal and chemical denaturation (Table 2).

The amino terminus of PFRD makes a main chain to side chain salt bridge with Glu 14. We used double mutant cycles

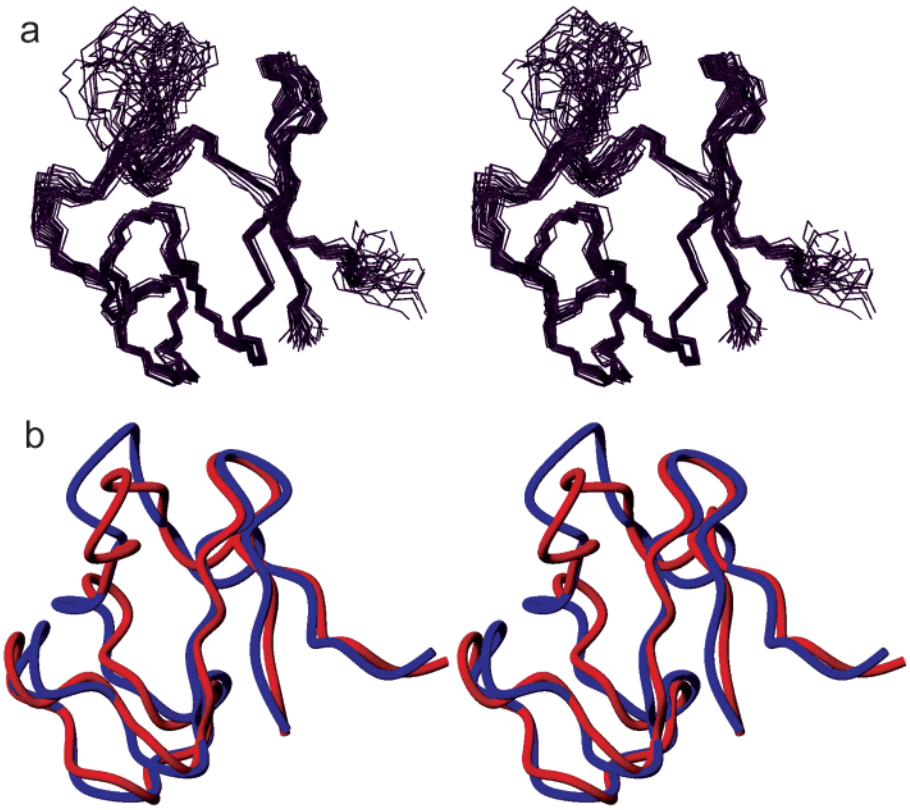

FIGURE 1: Stereoview of the PFRD-XC4 structure ensemble and comparison to the PFRD X-ray structure. (a) Best fit superposition of 28 simulated annealing structures. (b) Structural comparison of the PFRD (red) and PFRD-XC4 (blue) backbones. The region of greatest deviation is the minimally restrained loop of residues 37−45. Structure figures were generated using MOLMOL (*50*).

to isolate the stabilization effect of this interaction (*8*, *9*). The strength of interaction, $\Delta G^{XY}{}_{interaction}$, is calculated according to eq 1, where ΔG^{XY}, ΔG^{XA}, ΔG^{AY}, and ΔG^{AA} are the free energies of unfolding for the unmutated protein, the two singly mutated proteins, and the doubly mutated protein, respectively.

$$\Delta G^{XY}{}_{interaction} = (\Delta G^{XY} - \Delta G^{AA}) - [(\Delta G^{XA} - \Delta G^{AA}) + (\Delta G^{AY} - \Delta G^{AA})] \quad (1)$$

In mesophilic rubredoxins, methionine is retained at the N-terminus in contrast to the thermophile. The extended N-terminus is too far from the side chain of Glu 14 to form a salt bridge. To extend the N-terminus of the hyperthermophilic variant PFRD-XC4, residue 1 was mutated to a large amino acid (Gln), resulting in the retention of the N-terminal methionine. Mutants 14Q and 1Q14Q were also prepared to complete the double mutant cycle. Gln was selected at position 14 to disrupt any ionic interaction with the N-terminus while preserving the potential hydrogen bond to the N-terminus. Mutants 1Q, 14Q, and 1Q14Q were folded at room temperature, with T_m values reduced by 20−40 °C relative to that of PFRD-XC4 (Table 2).

Guanidinium chloride (GdmCl) chemical denaturations yielded the following free energies of unfolding: ΔG_u(PFRD-XC4) = 3.2 kcal mol^{-1}, ΔG_u(1Q) = 2.1 kcal mol^{-1}, ΔG_u(14Q) = 1.7 kcal mol^{-1}, and ΔG_u(1Q14Q) = 1.5 kcal mol^{-1} (Figure 3a). Due to the lack of well-defined pretransition baselines in the guanidinium chloride denaturation curves for mutants 14Q and 1Q14Q, the denaturation data were fit to a two-state model with a fixed pretransition slope. The pretransition slope was determined by averaging the pretransition slopes from seven separate PFRD-XC4 mutants. Little variation in the pretransition slopes was found among the seven PFRD-XC4 mutants, resulting in a ~0.1 kcal mol^{-1} error in the final fit of 14Q and 1Q14Q. On the basis of the guanidinium chloride-derived ΔG_u values of PFRD-XC4, 1Q, 14Q, and 1Q14Q (Table 2), the ionic component of the salt bridge between the N-terminus and Glu 14 stabilizes PFRD-XC4 by 0.9 kcal mol^{-1} (Table 3).

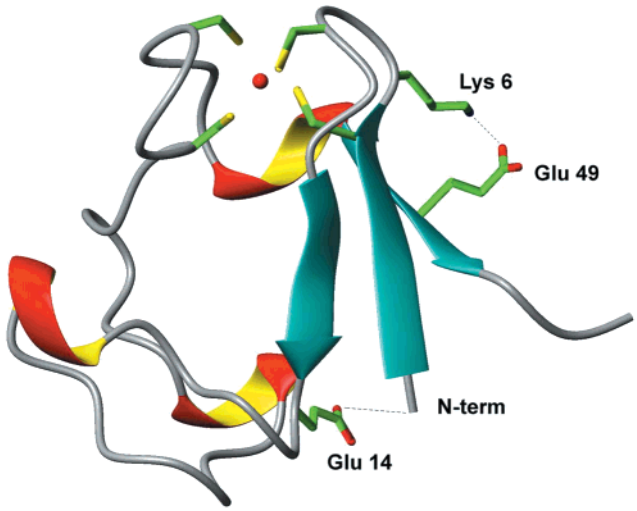

FIGURE 2: Ribbon diagram of wild-type *P. furiosus* rubredoxin showing the two salt bridges and the four cysteine residues that coordinate the iron.

Urea denaturations yielded the following free energies of unfolding: ΔG_u(PFRD-XC4) = 4.6 kcal mol^{-1}, ΔG_u(1Q)

Table 2: Thermal and Chemical Denaturation Data

protein	T_m[a] (°C)	ΔG_{GdmCl}[b] (kcal mol^{-1})	C_m[c] (M)	*m* value[d] (kcal mol^{-1} M^{-1})	ΔG_{urea}[e] (kcal mol^{-1})	C_m[f] (M)	*m* value[g] (kcal mol^{-1} M^{-1})
PFRD-XC4	82	3.2	1.68	1.9	4.6	5.7	0.81
PFRD-XC4-1Q	63	2.1	0.91	2.3	3.5	3.8	0.93
PFRD-XC4-14Q	57	1.7	0.63	2.5	2.7	3.0	0.91
PFRD-XC4-1Q14Q	39	1.5	0.50	3.0	2.1	2.0	1.03
PFRD-XC4-14T	38	–	–	–	1.3	1.3	0.98
PFRD-XC4-1Q14T	41	–	–	–	1.7	1.6	1.03
PFRD-XC4-6A	74	3.2	1.60	2.0	4.0	4.9	0.81
PFRD-XC4-49A	77	3.1	1.35	2.3	4.1	4.8	0.86
PFRD-XC4-6A49A	74	2.8	1.27	2.2	3.8	4.5	0.84

[a] Midpoint of thermal unfolding transition determined by CD. [b] Free energy of unfolding at 1 °C determined by GdmCl denaturations. [c] Midpoint of the GdmCl unfolding transition. [d] Slope of ΔG vs GdmCl concentration. [e] Free energy of unfolding at 1 °C determined by urea denaturations. [f] Midpoint of the urea unfolding transition. [g] Slope of ΔG vs urea concentration.

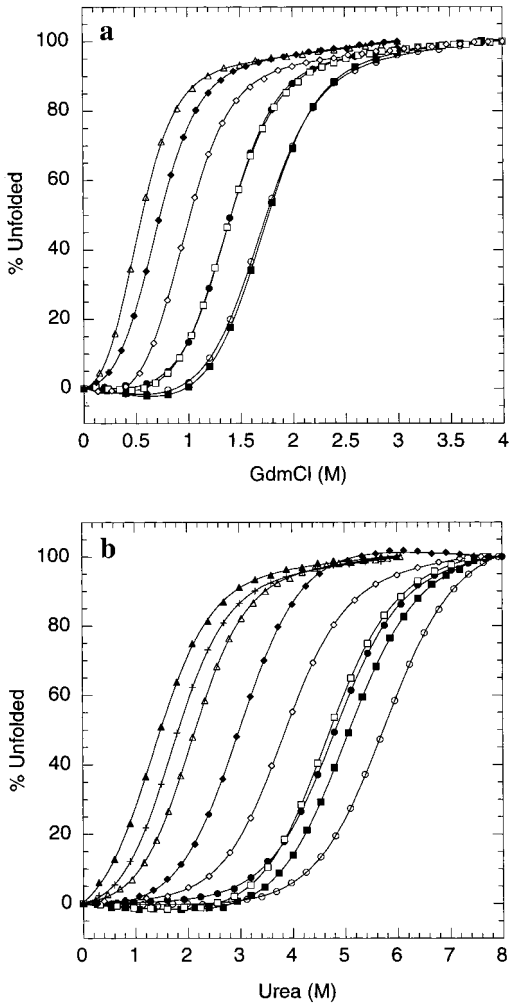

FIGURE 3: Chemical denaturation curves for PFRD-XC4 (○), 1Q (◇), 14Q (◆), 1Q14Q (△), 14T (+), 1Q14T (▲), 6A (■), 49A (●), and 6A49A (□) at 1 °C in (a) guanidinium chloride and (b) urea (to have the curves appear on the same plot, the initial and final points were arbitrarily called 0 and 100% unfolded despite the fact that proteins 14Q, 14T, 1Q14Q, and 1Q14T probably have an unfolded population even at 0% denaturant).

= 3.5 kcal mol^{-1}, ΔG_u(14Q) = 2.7 kcal mol^{-1}, and ΔG_u(1Q14Q) = 2.1 kcal mol^{-1} (Table 2). The urea denaturation data suggest that the ionic component of the N-terminal salt bridge stabilizes PFRD-XC4 by 0.5 kcal mol^{-1} (Table 3).

Mutants 14T and 1Q14T were designed to eliminate both the ionic and hydrogen bond components of the salt bridge between the N-terminus and Glu 14. GdmCl denaturations were not possible due to the low stability of these mutants. Urea denaturations yielded the following free energies of unfolding: ΔG_u(14T) = 1.3 kcal mol^{-1} and ΔG_u(1Q14TQ) = 1.7 kcal mol^{-1} (Figure 3b). On the basis of the urea denaturation data, the N-terminal salt bridge between the N-terminus and Glu 14 stabilizes PFRD-XC4 by 1.5 kcal mol^{-1}.

Table 3: Contributions of Salt Bridges at 1 °C

	Nt-E14 (ionic)[a] (kcal mol^{-1})	Nt-E14 (salt bridge)[b] (kcal mol^{-1})	K6-E49[c] (kcal mol^{-1})
GdmCl	0.9	–	−0.3
urea	0.5	1.5	0.3
average	0.7	1.5	0.0

[a] Ionic component of the interaction between the N-terminus and the side chain of residue 14. [b] Total salt bridge interaction between the N-terminus and the side chain of residue 14. [c] Total salt bridge interaction between side chains of residues 6 and 49.

The second salt bridge of interest in PFRD is formed by the side chains of Lys 6 and Glu 49. Mutants 6A, 49A, and 6A49A were created to disrupt this interaction. 6A, 49A, and 6A49A have melting temperatures lowered by only 5−9 °C relative to that of PFRD-XC4. The guanidinium chloride denaturation data (Table 2) do not show significant thermodynamic destabilization relative to PFRD-XC4: ΔG_u(PFRD-XC4) = 3.2 kcal mol^{-1}, ΔG_u(6A) = 3.2 kcal mol^{-1}, ΔG_u(49A) = 3.1 kcal mol^{-1}, and ΔG_u(6A49A) = 2.8 kcal mol^{-1}. The experimentally obtained $\Delta G_{interaction}$ for this salt bridge is −0.3 kcal mol^{-1} (Table 3). These data suggest that the side chain to side chain salt bridge between Lys 6 and Glu 49 in rubredoxin might be slightly destabilizing.

Urea denaturation data yield the following values: ΔG_u(PFRD-XC4) = 4.6 kcal mol^{-1}, ΔG_u(6A) = 4.0 kcal mol^{-1}, ΔG_u(49A) = 4.1 kcal mol^{-1}, and ΔG_u(6A49A) = 3.8 kcal mol^{-1} (Figure 3b). The urea denaturation data suggest that the salt bridge between Lys 6 and Glu 49 slightly stabilizes PFRD-XC4 by 0.3 kcal mol^{-1}. Taken together, the chemical and thermal denaturation data suggest that salt bridge between Lys 6 and Glu 49 has little effect on the stability of PFRD-XC4.

CONCLUSIONS

Theoretical and some experimental results suggest that forming a solvent-exposed ion pair may not be favorable, because in the process two ions have to be desolvated and immobilized (*9*, *12*, *14*, *44*−*47*). The surface salt bridge

between the side chains of Lys 6 and Glu 49, in which both side chains are immobilized, does not contribute to the overall stability of PFRD-XC4 at 1 °C and thus supports these findings. This salt bridge might play a role in setting the β-sheet register of rubredoxin or might be more stabilizing at higher temperatures (*48*). Previous reports have suggested that forming a salt bridge network might be stabilizing (*2*−*4*, *21*, *47*, *49*). In ion pair network formation after the first two residues are desolvated and immobilized, only one additional side chain needs to be desolvated and immobilized upon salt bridge formation, lowering the energetic cost. Forming a main chain to side chain salt bridge between the N-terminus and the side chain of Glu 14 in PFRD-XC4 stabilizes PFRD-XC4 by 1.5 kcal mol^{-1}. Main chain to side chain ion pairs may also have a lower formation cost, because the main chain is already fixed and only one additional residue must be immobilized. In PFRD-XC4, the N-terminus participates in the β-sheet and is immobilized. The main chain in PFRD-XC4 has already paid the immobilization entropy cost upon protein folding; thus, the energetic cost of forming a salt bridge to the N-terminus is significantly reduced in a manner similar to salt bridge formation in a surface ion pair network.

ACKNOWLEDGMENT

We thank M. K. Eidsness for the wild-type *P. furiosus* rubredoxin gene used in this study, S. Ross for NMR spectroscopy, and S. Ross and C. Sarisky for help with the NMR structure determination.

REFERENCES

1. Goldman, A. (1995) *Structure 3*, 1277−1279.
2. Yip, K. S., Stillman, T. J., Britton, K. L., Artymiuk, P. J., Baker, P. J., Sedelnikova, S. E., Engel, P. C., Pasquo, A., Chiaraluce, R., and Consalvi, V. (1995) *Structure 3*, 1147−1158.
3. Hennig, M., Darimont, B., Sterner, R., Kirschner, K., and Jansonius, J. N. (1995) *Structure 3*, 1295−1306.
4. Korndorfer, I., Steipe, B., Huber, R., Tomschy, A., and Jaenicke, R. (1995) *J. Mol. Biol. 246*, 511−521.
5. Day, M., Hsu, B., Joshua-tor, L., Park, J., Zhou, Z., Adams, M., and Rees, D. (1992) *Protein Sci. 1*, 1494−1507.
6. Perutz, M. F., and Raidt, H. (1975) *Nature 255*, 256−259.
7. Anderson, D. E., Becktel, W. J., and Dahlquist, F. W. (1990) *Biochemistry 29*, 2403−2408.
8. Horovitz, A., Serrano, L., Avron, B., Bycroft, M., and Fersht, A. R. (1990) *J. Mol. Biol. 216*, 1031−1044.
9. Serrano, L., Horovitz, A., Avron, B., Bycroft, M., and Fersht, A. R. (1990) *Biochemistry 29*, 9343−9352.
10. Kawamura, S., Tanaka, I., Yamasaki, N., and Kimura, M. (1997) *J. Biochem. 121*, 448−455.
11. Vetriani, C., Maeder, D. L., Tolliday, N., Yip, K. S., Stillman, T. J., Britton, K. L., Rice, D. W., Klump, H. H., and Robb, F. T. (1998) *Proc. Natl. Acad. Sci. U.S.A. 95*, 12300−12305.
12. Hendsch, Z. S., and Tidor, B. (1994) *Protein Sci. 3*, 211−226.
13. Honig, B., and Nicholls, A. (1995) *Science 268*, 1144−1149.
14. Matthews, B. W. (1993) *Annu. Rev. Biochem. 62*, 139−160.
15. Klump, H., Di Ruggiero, J., Kessel, M., Park, J. B., Adams, M. W., and Robb, F. T. (1992) *J. Biol. Chem. 267*, 22681−22685.
16. Wrba, A., Schweiger, A., Schultes, V., Jaenicke, R., and Zavodsky, P. (1990) *Biochemistry 29*, 7584−7592.
17. Laderman, K. A., Davis, B. R., Krutzsch, H. C., Lewis, M. S., Griko, Y. V., Privalov, P. L., and Anfinsen, C. B. (1993) *J. Biol. Chem. 268*, 24394−24401.
18. DeDecker, B. S., O'Brien, R., Fleming, P. J., Geiger, J. H., Jackson, S. P., and Sigler, P. B. (1996) *J. Mol. Biol. 264*, 1072−1084.
19. Pfeil, W., Gesierich, U., Kleemann, G. R., and Sterner, R. (1997) *J. Mol. Biol. 272*, 591−596.
20. Ogasahara, K., Lapshina, E. A., Sakai, M., Izu, Y., Tsunasawa, S., Kato, I., and Yutani, K. (1998) *Biochemistry 37*, 5939−5946.
21. Pappenberger, G., Schurig, H., and Jaenicke, R. (1997) *J. Mol. Biol. 274*, 676−683.
22. Cavagnero, S., Zhou, Z., Adams, M., and Chan, S. (1998) *Biochemistry 37*, 3377−3385.
23. Beadle, B. M., Baase, W. A., Wilson, D. B., Gilkes, N. R., and Shoichet, B. K. (1999) *Biochemistry 38*, 2570−2576.
24. Strop, P., and Mayo, S. L. (1999) *J. Am. Chem. Soc. 121*, 2341−2345.
25. Bau, R., Rees, D. C., Kurtz, D. M., Scott, R. A., Huang, H., Adams, M. W. W., and Eidsness, M. K. (1998) *JBIC, J. Biol. Inorg. Chem. 3*, 484−493.
26. Hemsley, A., Arnheim, N., Toney, M. D., Cortopassi, G., and Galas, D. J. (1989) *Nucleic Acids Res. 17*, 6545−6551.
27. Eidsness, M. K., Richie, K. A., Burden, A. E., Kurtz, D. M., Jr., and Scott, R. A. (1997) *Biochemistry 36*, 10406−10413.
28. Alexander, P., Fahnestock, S., Lee, T., Orban, J., and Bryan, P. (1992) *Biochemistry 31*, 3597−3603.
29. Johnson, B. H., and Hecht, M. H. (1994) *Bio/Technology 12*, 1357−1360.
30. Wüthrich, K. (1986) *NMR of Proteins and Nucleic Acids*, John Wiley and Sons, New York.
31. Piantini, U., Sorensen, O. W., and Ernst, R. R. (1982) *J. Am. Chem. Soc. 104*, 6800−6801.
32. Bax, A., and Davis, D. G. (1985) *J. Magn. Reson. 65*, 355−360.
33. Jeener, J., Meier, B. H., Bachmann, P., and Ernst, R. R. (1979) *J. Chem. Phys. 71*, 4546−4553.
34. Piotto, M., Saudek, V., and Sklenar, V. (1992) *J. Biomol. NMR 2*, 661−665.
35. Kraulis, P. J. (1989) *J. Magn. Reson. 24*, 627−633.
36. Bartels, C., Xia, T., Billeter, M., Guntert, P., and Wuthrich, K. (1995) *J. Biol. NMR 5*, 1−10.
37. Brünger, A. T. (1992) *X-PLOR, version 3.1, a system for X-ray crystallography and NMR*, Yale University Press, New Haven, CT.
38. Nilges, M., Clore, G. M., and Gronenborn, A. M. (1988) *FEBS Lett. 229*, 317−324.
39. Nilges, M., Kuszewski, J., and Brünger, A. T. (1991) in *Computational Aspects of the Study of Biological Macromolecules by NMR* (Hoch, J. C., Poulsen, F. M., and Redfield, C., Eds.) pp 451−457, Plenum Press, New York.
40. Kuszewski, J., Nilges, M., and Brunger, A. T. (1992) *J. Biol. NMR 2*, 33−56.
41. Minor, D. L., and Kim, P. S. (1994) *Nature 367*, 660−663.
42. Santoro, M. M., and Bolen, D. W. (1988) *Biochemistry 27*, 8063−8068.
43. Laskowski, R. A., Macarthur, M. W., Moss, D. S., and Thornton, J. M. (1993) *J. Appl. Crystallogr. 26*, 283.
44. Sun, D. P., Sauer, U., Nicholson, H., and Matthews, B. W. (1991) *Biochemistry 30*, 7142−7153.
45. Meeker, A. K., Garcia-Moreno, B., and Shortle, D. (1996) *Biochemistry 35*, 6443−6449.
46. Matthews, B. W. (1993) *Curr. Opin. Struct. Biol. 3*, 589−593.
47. Spek, E. J., Bui, A. H., Lu, M., and Kallenbach, N. R. (1998) *Protein Sci. 7*, 2431−2437.
48. Elcock, A. H. (1998) *J. Mol. Biol. 284*, 489−502.
49. Marqusee, S., and Sauer, R. T. (1994) *Protein Sci. 3*, 2217−2225.
50. Koradi, R., Billeter, M., and Wüthrich, K. (1996) *J. Mol. Graphics 14*, 51−55.

BI992257J